ELSEVIER

Journal of Atmospheric and Solar-Terrestrial Physics 69 (2007) 341–350

Journal of ATMOSPHERIC AND SOLAR-TERRESTRIAL PHYSICS

www.elsevier.com/locate/jastp

Two-dimensional drift velocities from the IMAGE EUV plasmaspheric imager

D.L. Gallagher[a,*], Mark L. Adrian[b]

[a]*NASA Marshall Space Flight Center, National Space Science & Technology Center, Mail Code VP62, 320 Sparkman Drive, Huntsville, AL 35805, USA*

[b]*NASA Goddard Space Flight Center Heliospheric Physics Branch Mail Code 612.2 Building 21, Room 254A, Greenbelt, MD 20771-1000, USA*

Received 5 April 2006; received in revised form 17 May 2006; accepted 23 May 2006
Available online 15 December 2006

Abstract

The Imager for Magnetopause-to-Aurora Global Exploration (IMAGE) Mission extreme ultraviolet (EUV) imager observes He^+ plasmaspheric ions throughout the inner magnetosphere. Limited by ionizing radiation and viewing close to the sun, images of the He^+ distribution are available every 10 min for many hours as the spacecraft passes through apogee in its highly elliptical orbit. As a consistent constituent at about 15%, He^+ is an excellent surrogate for monitoring all of the processes that control the dynamics of plasmaspheric plasma. In particular, the motion of He^+ transverse to the ambient magnetic field is a direct indication of convective electric fields. The analysis of boundary motions has already achieved new insights into the electrodynamic coupling processes taking place between energetic magnetospheric plasmas and the ionosphere. Yet to be fulfilled, however, is the original promise that global EUV images of the plasmasphere might yield two-dimensional pictures of mesoscale to macroscale electric fields in the inner magnetosphere. This work details the technique and initial application of an IMAGE EUV analysis that appears capable of following thermal plasma motion on a global basis.

Keywords: Plasmasphere; Convection; Electric fields; Plasmaspheric erosion

1. Introduction

Almost 10 years ago, Carpenter and Lemaire (1997) wrote that, "We see various effects of plasmasphere erosion through anecdotal data, without having direct global scale or mesoscale observations of the erosion process itself." The promise of global plasmaspheric imaging is to directly observe the whole system of plasmaspheric erosion and other inner magnetospheric processes. The Imager for Magnetopause-to-Aurora Global Exploration (IMAGE) is our community's first dedicated mission intended to fill this gap in our experimental knowledge of the inner magnetosphere (Burch, 2000). Observations using the IMAGE instrumentation have started to close the observational gap between the plasmasphere and ionosphere by finding the plasmaspheric plume in ionospheric

*Corresponding author. Tel.: +1 256 961 7687; fax: +1 256 961 7249.
E-mail address: dennis.l.gallagher@nasa.gov (D.L. Gallagher).

1364-6826/$ - see front matter © 2006 Elsevier Ltd. All rights reserved.
doi:10.1016/j.jastp.2006.05.028

observations (Foster et al., 2002), by finding subauroral polarization streams (SAPS) in the magnetosphere (Goldstein et al., 2003a), and by measuring field-aligned total densities that have permitted renewed study of the microphysics of plasmaspheric refilling (Reinisch et al., 2004).

While even the words we use to describe the plasmasphere have changed (Sandel et al., 2003), many of the physical processes that cause the observed behavior of thermal plasma remain obscure. For plasmaspheric physics and for ring-current ionosphere coupling, the exploration of mesoscale electric fields is a critical element and an area of active research (Goldstein et al., 2002; Khazanov et al., 2003; Gallagher et al., 2005; Liemohn and Brandt, 2005). In principle, a time sequence of global plasmaspheric density observations makes it possible to determine how plasma is moving regionally and to derive mesoscale electric fields. The most accessible form of this analysis is the study of major boundary motions. For example, Goldstein et al. (2004) have developed and applied this type of analysis to identifying the influence of the SAPS electric field on erosion of the westward edge of the plasmaspheric plume (see also Goldstein et al., 2003a). A limitation of the technique is that only the velocity component normal to the plasma density boundary can be obtained, yielding only the one-dimensional component of the electric field along the boundary. However the plasmapause motion is the integrated consequence of the motion of plasmaspheric plasma, which can be very different.

The objective of this investigation is to attempt a more general derivation of two-dimensional thermal He^+ plasma flow in the magnetic equatorial plane using observations of 30.4-nm scattered sunlight by the IMAGE extreme ultraviolet (EUV) imager (Sandel et al., 2000). Singly ionized helium is commonly about 15% of the proton composition of the plasmasphere (Craven et al., 1997) and an accepted surrogate of plasmaspheric densities. EUV is interpreted as being able to see the plasmasphere down to a total density of about $40\,cm^{-3}$ (Goldstein et al., 2003b) with a spatial resolution of about $0.1R_E$ at apogee (Sandel et al., 2000). Thermal plasma has long been known to have considerable structure, especially in the outer plasmasphere and beyond (Lemaire and Gringauz, 1998). The recent IMAGE observations by EUV and by the radio plasma imager (RPI) (Reinisch et al., 2000) have reinforced that conclusion, while at the same time revealing much more of the global morphology of plasmaspheric plasma.

The conclusion of this preliminary study of two-dimensional He^+ flow analysis in EUV observations is that it can be done and that previously inaccessible information about mesoscale plasma flows, and hence electric fields, may now enable entirely new advances in our understanding of inner magnetosphere coupling processes. As a preliminary study, most of this report is devoted to a discussion of the plasma flow analysis technique and the influence of experimental noise on its application. While the technique is not yet mature, it is proposed to be a viable and a powerful addition to our experimental investigation of magnetospheric processes through images.

2. Plasma drift analysis

The basic approach of this analysis is to identify local structure in images of the plasmasphere and quantify their drift from one image to the next. The assumption is that there is structure in the plasmaspheric density distribution that is often seen (e.g., Carpenter et al., 1993; Moldwin et al., 1994; Sandel, 2003) and that it will be possible to identify the same features in sequential images.

The movement of features in the field of view of an optical imager has received considerable attention. Two techniques have been considered for the analysis presented in this work. One technique is the calculation of optical flow (Horn and Schunck, 1981). Optical flow is determined by examining the spatial and temporal changes in intensity for each pixel in the field of view. The optical flow constraint equation is

$$-\frac{\partial I}{\partial t}=\frac{\partial I}{\partial x}\left(\frac{\partial x}{\partial t}\right)+\frac{\partial I}{\partial y}\left(\frac{\partial y}{\partial t}\right), \quad (1)$$

where I is intensity and (x,y) the spatial position in the field of view. This equation requires the assumption that the brightness of the image is not otherwise changing. Constraints can also be applied to the rate of change of derived flow in space and in time if smoothness in either can be assumed. An attempt to make use of this technique with IMAGE EUV images has been made by Christophe Bernard (private communication) at the École Polytechnique in France. An Interactive Data Language version of his code can be obtained from Belgium where it has been translated from the original Matlab language (http://csrsrv1.fynu.ucl.ac.be/csr_web/data/) by

Juan Cabrera at the Center for Space Radiations. The initial use of this optical flow code for this study was not successful; however, it is too soon to discount its use.

Another technique for matching features from one image to the next is by cross-correlation analysis. For this technique, a kernel representing a portion of the first image is differenced with the same sized portion or subimage of a subsequent image to determine a correlation coefficient or quality of correspondence. Cross-correlation coefficients are calculated across a range of subimages until the best match is found or it is determined that no match of sufficient quality can be found. Fig. 1 graphically illustrates the technique. The following equation provides the mathematical formalism:

$$CC(i,j)_{m,n} = \frac{\sum_{k,l}(n_K(k,l)i,j - n_s(k,l)_{m,n})^2/n_K}{N}, \quad (2)$$

where $CC(i,j)_{m,n}$ is the correlation coefficient for the (i,j) kernel when correlated with a subarray from the next image at the (m,n) position. The summation is over the (k,l) elements within the kernel and subarray. The symbols n_K and n_S represent the densities in the kernel and subarray, since what is sought is a correlation between the density distributions of plasmaspheric He^+ from one image to the next. It should be noted that any drift will be finite in speed; therefore, the locations at which the cross correlation is computed for a given kernel can be

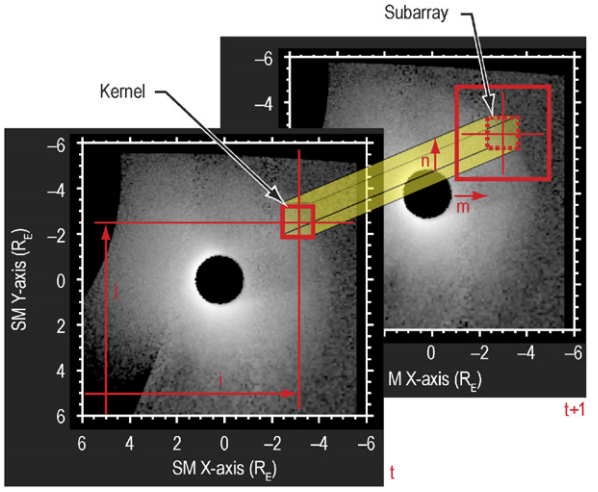

Fig. 1. The cross-correlation procedure for determining drift in EUV images is shown graphically. Each panel shows pseudodensity in the solar magnetic equatorial plane derived from sequential EUV images. Pseudodensity increases logarithmically with increasing gray-scale intensity. The dark center is the location of the Earth. The sun is to the left.

limited. The equatorial density distribution of He^+ observed by EUV can be obtained for each image by a full inversion (Gurgiolo et al., 2005) or as done for this initial study where pseudodensity is used (Gallagher et al., 2005). Pseudodensity is a determination of equatorial He^+ density from an EUV image where some of the geometric observing effects have been removed and it is assumed that most of the image intensity derives from the innermost L-shells along each pixel's line of sight. Each panel in Fig. 1 shows pseudodensity in the solar magnetic equatorial plane derived from sequential EUV images. A gray-scale is used to represent pseudodensity values with higher densities shown as brighter shading.

In principle, an optimum cross-correlation can be computed for each kernel position and thereby drift speeds, generally across the EUV field of view in a sequence of images, can be derived. Not all variations in EUV image content correspond to features in the distribution of plasmaspheric He^+. A single image from EUV is actually composed of three images from separate cameras (Sandel et al., 2000). The flat-field correction and composition of the separate images sometimes leaves artifacts in an image along the "seams" between cameras. Each camera is independently capable of protecting itself from the sun and solar reflections. That happens by a lowering of the detector high voltage and a roll-off in image intensity. The pseudodensity shown in Fig. 1 suffers from this effect in the lower left corner. A gradual turning on or off of a camera's high voltage can also lead to a perceived flow of plasma in an automated correlation analysis computer program, and that must be guarded against. A prominent feature of EUV images is noise that tends to hide the plasmaspheric structures needed for this drift analysis.

3. The influence of noise

EUV image noise strongly influences the character of acquired images of plasmaspheric He^+ and the correlation coefficient analysis of image pairs. Fig. 2 is an example of how noise manifests itself in this analysis. Two sequential 10-min integrated EUV images are used for the cross-correlation calculation. The first image is centered at 0545 UT and the second at 0555 UT on July 10, 2000. The pseudodensity at 0555 UT is shown in gray-scale in the figure. Red arrows are used to indicate derived plasma flow, where the legend here and in other figures defines the arrow length scaling. It is

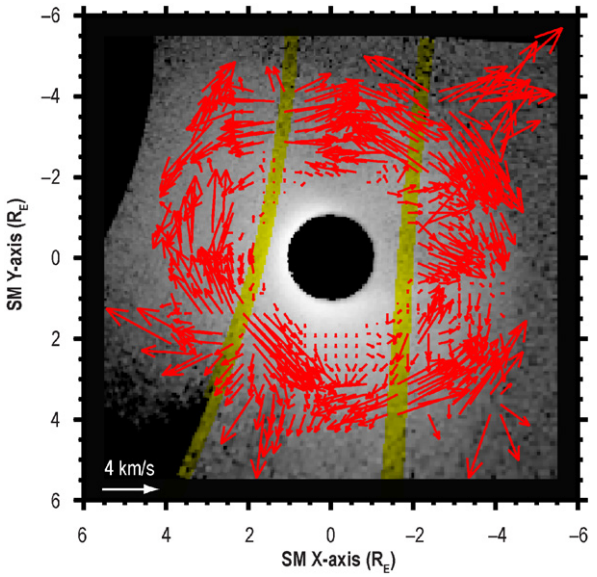

Fig. 2. Cross-correlation-derived drifts are shown by red arrows. Two sequential 10-min integrated EUV images are used in the analysis, ending with the one shown at 0555 UT on July 10, 2000. The yellow shading shows where instrument imaging head observations overlap.

interesting to point out that the dominant pattern of divergent and convergent arrows is well organized by the overlaid yellow bands. The yellow regions mark the overlap between individual EUV imaging sensors; hence, the obtained flow pattern without noise mitigation seems more related to the sensor geometry and properties than to the physical behavior of the imaged plasma. It is expected that noise may play a role in obscuring plasma flow. The challenge is in reducing noise without eliminating evidence of density structure in the underlying image.

In this initial study, a median filter for noise mitigation is used that is $1R_E \times 1R_E$ in spatial size. A median filter replaces each pixel by the median value in the field of consideration and is known for preserving edges in images better than linear smoothing filters, such as the Hann, Butterworth or Gaussian filters (see the discussion and citations in Hannequin and Max, 2002). A relatively large median filter box size was necessary to usefully reduce the influence of noise on the flow analysis. The large size also tends to increase the smoothing effect of the technique, although not as much as the linear smoothing filters. Several filters have been tried to this point. These include boxcar smoothing, the Lee filter (Lee, 1986), Fourier transform spatial frequency filtering, and Wavelet transform filtering. None of these other filters performed better and most performed worse than the median filter.

Fig. 3 shows the same flow analysis as that performed for Fig. 2 after a median filter has been applied to the pseudodensities from each image. The change is dramatic even though a median filter is not expected to be the best choice for EUV images, and, in fact, there remain features in the derived flow that still appear to be artificial. A better treatment of noise is expected from a technique that is based on the properties of Poisson and additive noise, as briefly discussed below. As will be shown in the next section, the divergent postmidnight flow (highlighted by the yellow oval in Fig. 3) appears to be real, showing plasmaspheric erosion flows at an early stage.

Noise in EUV images has at least three sources. Photon counting leads to Poisson noise, microchannel plate noise is additive and radiation noise is also additive. Poisson noise appears to be particularly challenging to remove in photon images. Two techniques appear to offer improved Poisson noise removal but remain to be studied in subsequent work. The first is a technique presented by Hannequin and Max (2002) and the second by Le et al. (2005). The objective of both techniques is to remove Poisson noise while retaining the underlying

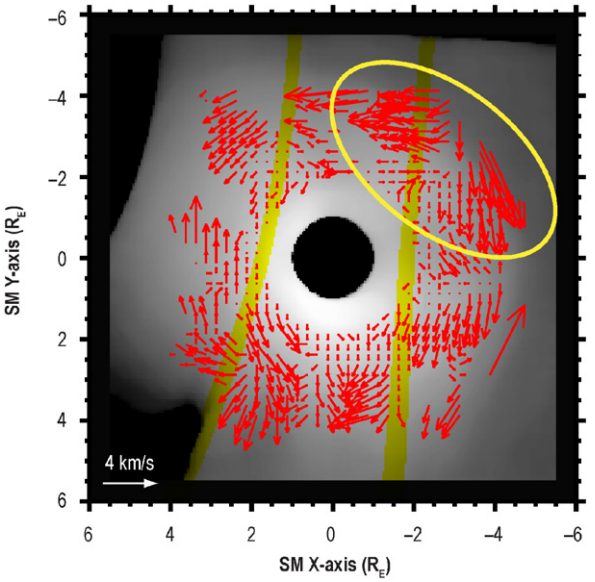

Fig. 3. Drift velocities are again derived for 0555 UT on July 10, 2000, except that in this case noise has been reduced by use of a median filter. The yellow oval locates a region of divergent flow that appears to be real.

structure characteristic of the imaged object. A more sophisticated treatment of noise mitigation and a rigorous testing of the recovery of plasma drift using the cross-correlation analysis have been initiated and will be presented in a later manuscript.

Ultimately, the use of derived drift velocities depends on the errors inherent in the analysis. Figs. 4 and 5 are provided to illustrate a typical cross-correlation analysis. Fig. 4 shows the derivation of a single flow vector (shown as a red arrow) centered at solar magnetic coordinates $(x,y) = (-3.1, -1.9R_E)$. The shading around the arrow indicates the kernel size and the region across which the correlation analysis is performed. The graphic insert shows the correlation values below 0.01 in reverse gray scale, where the best (lowest) value location is indicated by the red dot. The blue dot indicates the location along the ridge where the smallest drift velocity is located and is provided for reference. Should the correlation array fail to indicate a clear best fit, one alternative would be to choose the least drift consistent with the analysis; however, that option is not used in any of the analysis presented in this work. Note the orientation of the ridge of best correlation values. Typically, plasmaspheric densities fall strongly with increasing distance from the Earth, often with limited structure in the azimuthal direction. The ridge orientation is generally perpendicular to the radial direction, consistent with the expectation of greater (lesser) variation in correlation values in the radial (azimuthal) direction. The ridge reduces to a small irregular region where the plasmasphere is strongly structured, such as at the westward base of the plume.

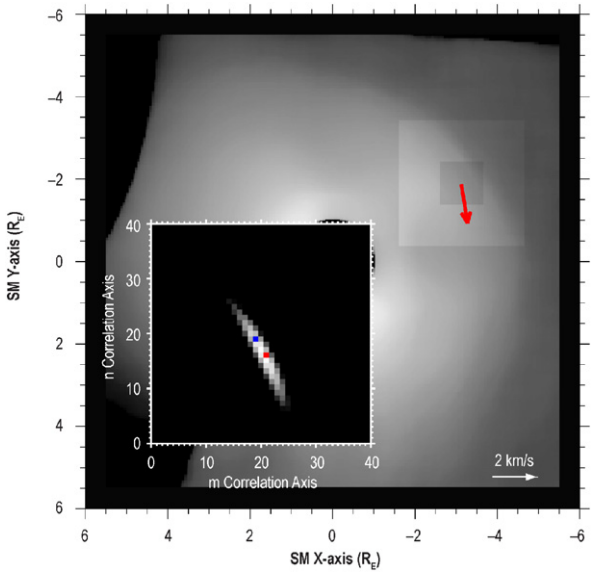

Fig. 4. The flow vector at 0555 UT and solar magnetic $(x,y) = (-3.1,-1.9)R_E$ is shown in red. The shading around the arrow indicates the kernel size and the region across which the correlation analysis is performed. The graphic insert shows the correlation values below 0.01 in reverse gray scale, where the best value location is indicated by the red dot. The blue dot indicates that location along the ridge where the smallest drift velocity is located.

Fig. 5 shows the correlation values along and transverse to the ridge of best values shown in the Fig. 4 insert. The values along the ridge are shown in the left panel. The red curve is a Gaussian fit to the values below 0.01 and the red line marks the center of the fitted curve. The red and blue asterisks correspond to the best correlation value and the one along the ridge of best values requiring the least drift, respectively. The values transverse to the ridge of best values, shown on the right, are chosen to pass through the Gaussian fit location shown on the left. The red curve is a Gaussian fit to the best five transverse values and the red line marks the center of the fitted curve. The blue line marks the best correlation value along this transverse path. Only a few values near the centerline of the ridge are chosen for the Gaussian fit due to the asymmetric profile of the correlation values. As more values are used in the fit, the Gaussian fit is clearly drawn from the correct solution. This asymmetric shape is common and consistent with the preceding discussion of the sensitivity of correlation values to plasmaspheric density gradients, which reduce with increasing radial distance.

Along and transverse to the ridge of best correlation values, the derived drift velocities are 1.77 ± 0.11 and -0.43 ± 0.26 km/s, respectively, for a total drift velocity of about 1.9 km/s. At this location, the strength of the dipole magnetic field can be used to estimate a net convective electric field of 1.2 mV/m. Goldstein et al. (2003c) have derived a time varying azimuthal electric field corresponding to the inward, radial plasmapause motion during this event. At 0555 UT, they obtain a westward electric field of about 0.9 mV/m. The flow velocity vector shown in Fig. 4 is nearly azimuthal rather than radial and is neither the weakest nor strongest derived by this flow analysis. To make a direct comparison between this flow analysis and the plasmapause motion analysis of Goldstein et al. (2003c), it would be necessary to derive the resulting rate of erosion of the plasmasphere brought about

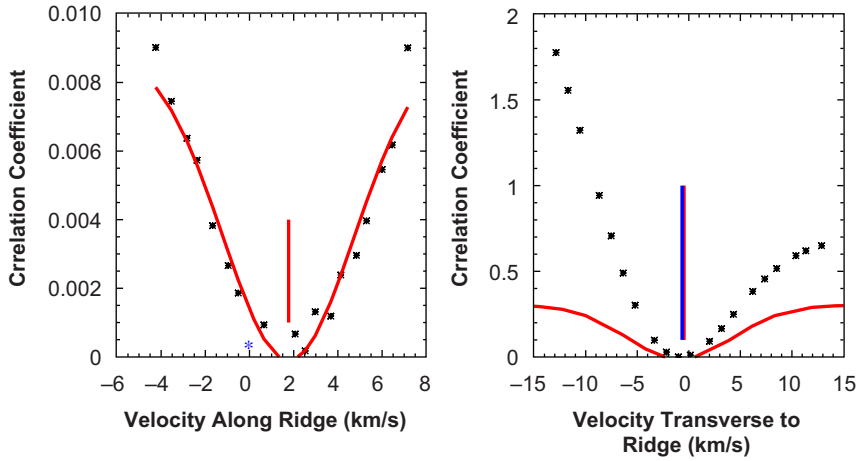

Fig. 5. The correlation values along and transverse to the ridge-of-best-values shown in Fig. 4 are plotted. The values along the ridge are shown in the left panel. The red curve is a Gaussian fit to the values below 0.01 and the red line marks the center of the fitted curve. The red and blue asterisks correspond to the best correlation value and the one along the ridge-of-best-values requiring the least drift, respectively. The values transverse to the ridge-of-best-values, shown on the right, are chosen to pass through the Gaussian fit location shown on the left. The red curve is a Gaussian fit to the best five values and the red line marks the center of the fitted curve. The blue line marks the best correlation value along this transverse path.

by the flows found here. While that analysis is outside the scope of the present work, it is useful to note that the electric-field strengths that can be inferred from the derived flow velocities are comparable to those derived by an independent technique.

4. One plasmaspheric erosion event

The erosion event of July 10, 2000 has previously been studied by Goldstein et al. (2003c). In that work, the details of solar-wind electric field are compared successfully with motion of the plasmapause during the erosion process. A southward turning of the interplanetary magnetic field (IMF) Bz along with subsequent changes in the solar-wind imposed electric field are reasonably well correlated with the pattern of inward movement of the plasmapause given a 30 min time delay. This event has been chosen for the initial application of EUV plasma flow analysis because it is well observed by the imager and because the conditions and plasmaspheric response have already been characterized.

The focus here is on the postmidnight-to-dawn quadrant during the onset of erosion. Fig. 3 of Goldstein et al. (2003b) shows the solar-wind electric field abruptly going negative just prior to 0500 UT on this day. It stays negative with a smaller positive jump at about 0600 UT. Fig. 6 in this study displays the plasmaspheric flow pattern in the vicinity of the plasmapause from 0454 to 0616 UT. As before, the red arrows indicate He^+ flow. The yellow arrows in each panel indicate the approximate location from which the flow appears to diverge. Westward of this location, the flow is inward and westward. Eastward of this location, the flow is inward and eastward. This is the same location at which a subtle inward "dimple" appears and moves dawnward, similar to the more pronounced shoulder feature previously reported (Goldstein et al., 2002). What appear to be counter-rotating flows are similar to that presented by Gallagher et al. (2005), based on the numerical results of Liemohn et al. (2004) and Liemohn and Brandt (2005), where injected plasmasheet particles develop paired pressure peaks and drive counter-rotating $\mathbf{E} \times \mathbf{B}$ flows. This potential structure was suspected to cause outward flow of plasmaspheric plasma at evening local times, developing a plasmaspheric prominence. A reversed polarity of the pressure peaks would lead to an inward flow and circulation of thermal ions as is seen in Fig. 6. The derived inward and azimuthal motion of thermal plasma appears to be the manifestation of the penetrating electric field that is driving erosion of the outer plasmasphere during this event. The apparent origin of the divergent flow

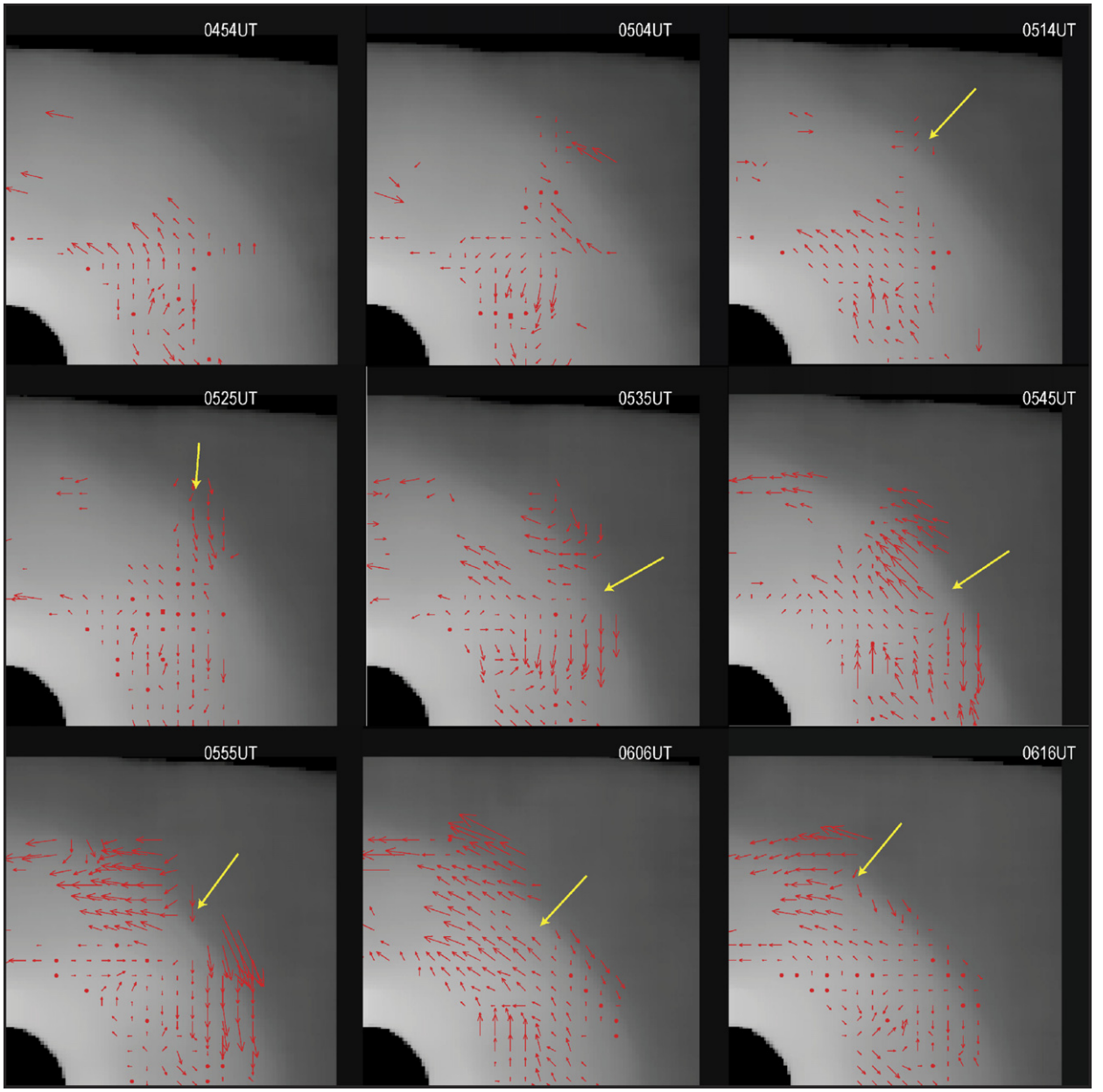

Fig. 6. Plasmaspheric drift during onset of the erosion event of July 10, 2000 is shown in the midnight to dawn sector. The red arrows indicate He^+ flow and the yellow arrows indicate the approximate point from which the flow diverges. The spatial scale extends from 0 to $6R_E$ in the negative solar magnetic x and y-axis directions.

moves dawnward systematically after 0535 UT. For the first 50 min, this location moves at ~3.5 h in MLT per hour of universal time. As the event proceeds, a divergent flow is replaced by a persistent sunward and eastward flow that can be seen until about 0800 UT when progressive shut down of one of the EUV imager heads, due to sunlight contamination, interrupts the flow analysis.

5. Discussion and summary

The objective of this investigation is to develop a technique for using IMAGE EUV observations to

derive two-dimensional thermal plasma flow in the magnetic equatorial plane. The boundaries of the plasmapause and plasmaspheric plume are not the only features of thermal plasma density distribution seen by EUV, but they are the most clear and easiest to follow through time. Initial analysis of these boundary motions has already established the value of EUV-derived electric fields to test theoretical and numerical modeling of inner magnetospheric processes (e.g., Goldstein et al., 2005). Knowledge of equatorial thermal plasma flow velocities across major regions of the inner magnetosphere enables a much more complete examination of the coupling between energetic and thermal magnetospheric plasma and the ionosphere during all phases of storms and substorms through recovery.

Plasmaspheric erosion on July 10, 2000 is preliminarily found to be initiated near 3 h MLT and is characterized by divergent flows that appear responsible for the inward motion of the plasmapause. Westward flows away from the initial erosion site are not yet well obtained; however, an eastward flow into midmorning local times is followed for 2–3 h. It remains to be determined whether this erosion event is characteristic of all plasmaspheric erosion events or whether the complete morphology of plasmaspheric erosion, recovery and the development of the other observed plasmaspheric density structures, such as "fingers" (Adrian et al., 2004), can be revealed by EUV plasma flow analysis.

The median filter employed in this analysis did not remove all derived flows attributed to noise. The plasmasphere does not, in all regions, appear to have density structure that can be followed from one image to the next. It can be expected that any analysis of plasma flow with EUV will necessitate a skeptical interpretation of what is found, most often dependent on finding systematic and coherent time evolving flows before results can be believed. Much plasmaspheric structure is known to exist below the EUV sensitivity at low densities and into the outer magnetosphere (e.g., Moldwin et al., 1994; LeDocq et al., 1994; Carpenter and Lemaire, 1997; Carpenter et al., 2000). In all however, the initial success from the flow analysis presented here seems a clear indication that much is yet to be gained from IMAGE Mission observations and from better imaging technology in the future.

Ring-current plasma is expected to be a source of mesoscale electric field structure (Goldstein et al., 2002; Khazanov et al., 2003; Gallagher et al., 2005; Liemohn and Brandt, 2005). Two features dominate the postmidnight plasma flows. The first is the divergent flow pattern seen for about 50 min during the event. The second is motion of the center that flows westward, much like what might be expected of energetic drifting particles. For a given energy, the drift velocity for energetic particles will be a combination of corotation, gradient curvature and $\mathbf{E}\times\mathbf{B}$ drift resulting from the local convection electric field. If it is assumed the westward drift of the divergent flow pattern results from drifting energetic particles, then the derived total corotation and convective electric field can be used to estimate their energy.

Focus again on the drift velocities obtained between the EUV observations at 0545 and 0555 UT which are shown in Fig. 3. The eastward drifts east of the divergent point are largely in the region of $-3.0<\mathrm{Xsm}<-1.0$ and $-4.0<\mathrm{Ysm}<-3.0$. The average location for the drift velocities recovered from this region has a radial distance of $4.0R_{\mathrm{E}}$ and an average drift velocity magnitude (mostly eastward) of 2.85 km/s. This translates to 1.5 MLT h/UT hour at $L=4$, which is much less than the observed drift in the divergent pattern. The observed drift of the divergent location of 3.5 MLT h/UT hour minus 1.5 MLT h/UT hour for the derived plasmaspheric corotation and mesoscale convective drift leaves about 2.0 MLT h/UT hour of drift to be accounted for by gradient-curvature drift. The corresponding drift frequency is about 0.02 mHz, and, for $L=4$, it is found that particles with an energy of about 13 keV would be consistent with the drifting center of divergent flow, using Fig. 6 from Schulz and Lanzerotti (1974). This is a reasonable energy for injected ring-current particles and a starting point for subsequent investigation of the importance of ring-current-generated mesoscale electric fields to plasmaspheric erosion.

It is the conclusion of this study that it is possible to use EUV observations to determine plasmaspheric flow throughout large regions of the inner plasmasphere. However, the "path" is not entirely clear of problems. A major obstacle not yet fully resolved is the influence of noise in EUV images. Given that a simplistic treatment of noise with a median filter results in what has been presented here, a more robust treatment of Poisson, detector and radiation noise should be expected to yield an even clearer picture of thermal plasma flow.

Acknowledgments

This research was supported by the IMAGE Mission through the NASA Science Mission Directorate. The author particularly acknowledges access to the IMAGE/EUV observations through the University of Arizona website at http://euv.lpl.arizona.edu/euv/ and the insight about the instrument gained by discussions with Dr. Bill Sandel and Mr. Terry Forrester. This work has benefited from discussion of noise removal and image feature tracking with Dr. Timothy Newman who is in the Computer Science Department of the University of Alabama in Huntsville.

References

Adrian, M.L., Gallagher, D.L., Avanov, L.A., 2004. IMAGE EUV observation of radially, bifurcated plasmaspheric features: first observations of a possible standing ULF waveform in the inner magnetosphere. Journal of Geophysical Research 109 (A1), A01203.

Burch, J.L., 2000. IMAGE mission overview. Space Science Reviews 91, 1–14.

Carpenter, D.L., Lemaire, J., 1997. Erosion and recovery of the plasmasphere in the plasmapause region. Space Science Reviews 80, 153–179.

Carpenter, D.L., Giles, B.L., Chappell, C.R., Decreau, P.M.E., Anderson, R.R., Persoon, A.M., Smith, A.J., Corcuff, Y., Canu, P., 1993. Plasmasphere dynamics in the duskside bulge region: a new look at an old topic. Journal of Geophysical Research 98, 19,243.

Carpenter, D.L., Anderson, R.R., Calvert, W., Moldwin, M.B., 2000. CRRES observations of the density cavities inside the plasmasphere. Journal of Geophysical Research 105, 23,323–23,338.

Craven, P.D., Gallagher, D.L., Comfort, R.H., 1997. Relative concentration of $He+$ in the inner magnetosphere as observed by the DE 1 retarding ion mass spectrometer. Journal of Geophysical Research 102, 2279–2289.

Foster, J.C., Erickson, P.J., Coster, A.J., Goldstein, J., Rich, F.J., 2002. Ionospheric signatures of plasmaspheric tails. Geophysical Research Letters 29 (13).

Gallagher, D.L., Adrian, M.L., Liemohn, M.W., 2005. The origin and evolution of deep plasmaspheric notches. Journal of Geophysical Research 110, A09201.

Goldstein, J., Spiro, R.W., Reiff, P.H., Wolf, R.A., Sandel, B.R., Freeman, J.W., Lambour, R.L., 2002. IMF-driven over shielding electric field and the origin of the plasmaspheric shoulder of May 24, 2000. Geophysical Research Letters 29.

Goldstein, J., Sandel, B.R., Hairston, M.R., Reiff, P.H., 2003a. Control of plasmaspheric dynamics by both convection and Sub-Auroral Polarization Stream. Geophysical Research Letters 30 (24), 2243.

Goldstein, J., Spasojevic, M., Reiff, P.H., Sandel, B.R., Forrester, W.T., Gallagher, D.L., Reinisch, B.W., 2003b. Identifying the plasmapause in IMAGE EUV data using IMAGE RPI in situ steep density gradients. Journal of Geophysical Research 108 (A4), 1147.

Goldstein, J., Sandel, B.R., Forrester, W.T., Reiff, P.H., 2003c. IMF-driven plasmasphere erosion of 10 July 2000. Geophysical Research Letters 30.

Goldstein, J., Wolf, R.A., Sandel, B.R., Reiff, P.H., 2004. Electric fields deduced from plasmapause motion in IMAGE EUV images. Geophysical Research Letters 31, L01801.

Goldstein, J., Burch, J.L., Sandel, B.R., Mende, S.B., Brandt, P.C:son, Hairston, M.R., 2005. Coupled response of the inner magnetosphere and ionosphere on 17 April 2002. Journal of Geophysical Research 110, A03205.

Gurgiolo, C., Sandel, B.R., Perez, J.D., Mitchell, D.G., Pollock, C.J., Larsen, B.A., 2005. Overlap of the plasmasphere and ring current: relation to subauroral ionospheric heating. Journal of Geophysical Research 110, A12217.

Hannequin, P., Max, J., 2002. Statistical and heuristic image noise extraction (SHINE): a new method for processing Poisson noise in scintigraphic images. Physics in Medicine and Biology 47, 4329–4344.

Horn, B.K.P., Schunck, B.G., 1981. Determining optical flow. Artificial Intelligence 17, 185–203.

Khazanov, G.V., Liemohn, M.W., Newman, T.S., Fok, M.-C., Spiro, R.W., 2003. Self-consistent magnetosphere-ionosphere coupling: theoretical studies. Journal of Geophysical Research 108.

LeDocq, M.J., Gurnett, D.A., Anderson, R.R., 1994. Electron number density fluctuations near the plasmapause observed by the CRRES spacecraft. Journal of Geophysical Research 99, 23,661–23,671.

Le, T., Chartrand, R., Asaki, T.J., 2005. A variational approach to reconstructing images corrupted by Poisson noise. UCLA CAM Report 05-49.

Lee, J.-S., 1986. Speckle suppression and analysis for synthetic aperture radar images. Optical Engineering 25 (5), 636–646.

Lemaire, J.F., Gringauz, K.I., 1998. The Earth's Plasmasphere. Cambridge University Press, Cambridge.

Liemohn, M.W., Brandt, P.C., 2005. Small-scale structure in the storm time ring current, in inner magnetosphere interactions: new perspectives from imaging. In: Burch, J.L., Schulz, M., Spence, H. (Eds.), American Geophysical Union AGU Monographs 159, vol. 167.

Liemohn, M.W., Ridley, A.J., Gallagher, D.L., Ober, D.M., Kozyra, J.U., 2004. Dependence of plasmaspheric morphology on the electric field description during the recovery phase of the April 17, 2002 magnetic storm. Journal of Geophysical Research 109 (A3), A03209.

Moldwin, M.B., Thomsen, M.F., Bame, S.J., McComas, D.J., Moore, K.R., 1994. An examination of the structure and dynamics of the outer plasmasphere using multiple geosynchronous satellites. Journal of Geophysical Research 99, 11,475–11,481.

Reinisch, B.W., Haines, D.M., Bibl, K., Cheney, G., Galkin, I.A., Huang, X., Myers, S.H., Sales, G.S., Benson, R.F., Fung, S.F., Green, J.L., Boardsen, S., Taylor, W.W.L., Bougeret, J.-L., Manning, R., Myer-Vernet, N., Moncuquet, M., Carpenter, D.L., Gallagher, D.L., Reiff, P., 2000. The radio plasma imager investigation on the IMAGE spacecraft. Space Science Reviews 91, 319–359.

Reinisch, B.W., Huang, X., Song, P., Green, J.L., Fung, S.F., Vasyliunas, V.M., Gallagher, D.L., Sandel, B.R., 2004.

Plasmaspheric mass loss and refilling as a result of a magnetic storm. Journal of Geophysical Research 109 (A1), A01202.

Sandel, B.R., Broadfoot, A.L., Curtis, C.C., King, R.A., Stone, T.C., Hill, R.H., Chen, J., Siegmund, O.H.W., Raffanti, R., Allred, D.D., Turley, R.S., Gallagher, D.L., 2000. The extreme ultraviolet imager investigation for the IMAGE mission. Space Science Reviews 91, 197–242.

Sandel, B.R., Goldstein, J., Gallagher, D.L., Spasojevic, M., 2003. EUV observations of the structure and dynamics of the plasmasphere. Space Science Reviews 109 (1–4), 25–46.